Photodissociation and Electronic Spectroscopy of $Mn(H)(CO)_3(H\text{-}DAB)$ (DAB = 1,4-Diaza-1,3-butadiene): Quantum Wave Packet Dynamics Based on ab Initio Potentials

Dominique Guillaumont and Chantal Daniel*

Contribution from the Laboratoire de Chimie Quantique UMR 7551, CNRS/Université Louis Pasteur, Institut Le Bel, 4 Rue Blaise Pascal, 67 000 Strasbourg, France

Received June 17, 1999. Revised Manuscript Received October 6, 1999

Abstract: The photodissociation dynamics of $Mn(H)(CO)_3(H\text{-}DAB)$ have been studied through wave packet propagations on CASSCF/MR-CCI potentials calculated for the electronic ground and low-lying excited states as a function of two coordinates q_a and q_b corresponding to the Mn−H bond homolysis and to the axial CO loss, respectively. The theoretical absorption spectrum is characterized by two bands, one intense peak centered at 476 nm (21 000 cm^{-1}) and one broad band centered at 285 nm (35 000 cm^{-1}). The visible band has been assigned to the low-lying metal-to-ligand charge-transfer (MLCT) states with a main contribution of the $a^1A' \rightarrow c^1A'$ transition corresponding to the $3d_{xz} \rightarrow \pi^*_{DAB}$ excitation. The second band calculated in the UV energy domain has been assigned to the d^1A' ($3d_{yz} \rightarrow 3d_{xy}$) and e^1A' ($\sigma_{Mn-H} \rightarrow \pi^*_{DAB}$) states corresponding to a metal-centered (MC) and a σ-bond-to-ligand charge-transfer (SBLCT) state, respectively. Simulation of excited states dynamics upon visible irradiation by propagation of selected wave packets on the two-dimensional MLCT potentials coupled nonadiabatically indicates a probability of dissociation of the axial CO of 99% in 400 fs. Nonradiative transitions to the low-lying triplet states or homolysis of the metal−hydrogen bond via the dissociative ^{3}SBLCT state are not competitive with this ultrafast deactivation process. Simulation of the UV photochemistry points to a very low probability of dissociation in this energy region.

I. Introduction

According to a number of recent experimental studies,[1−6] $MR(CO)_3$(α-diimine) complexes (in which M = Mn or Re, and R represents a metal fragment or alkyl or halide groups bound to the metal by a high-lying σ_{M-R} orbital) follow a variety of deactivation mechanisms after irradiation in the visible region (λ = 500 nm) depending on the metal center, on the nature of the radical R, and on the type of α-diimine ligand. The photochemical reactions currently observed for manganese complexes are either the homolytic rupture of the Mn−R bond, or the carbonyl loss,

$$M(R)(CO)_3(\alpha\text{-diimine}) \xrightarrow{h\nu} {}^{\bullet}M(CO)_3(\alpha\text{-diimine}) + {}^{\bullet}R \quad \text{(i)}$$

$$M(R)(CO)_3(\alpha\text{-diimine}) \xrightarrow{h\nu} M(R)(CO)_2(\alpha\text{-diimine}) + CO \quad \text{(ii)}$$

These two primary reactions lead to the formation of unsaturated primary products with quantum yields which depend on the ligand R (ϕ_{CO} = 1.0 for R = benzyl and ϕ_{CO} = 0.6 for R = methyl).[7,8] In contrast, the rhenium complexes show either radicals formation (reaction i) or intense emissions indicating the presence of long-lived time excited-states precursors of electrons/energy-transfer processes. The quantum yield of the Re−R bond homolysis increases on going from R = methyl to R = ethyl or benzyl.[9−11]

To rationalize the experimental data, several theoretical investigations, based either on DFT calculations[12−14] or on accurate CASSCF/MR-CCI studies,[15−18] have been performed. It has been shown that the three-center interaction between the group R (R = H, methyl or ethyl), the metal atom (M = Mn or Re), and the low-lying π^*_{H-DAB} acceptor ligand controls entirely the photochemical and photophysical properties of this class of

(1) Stufkens, D. J. *Comments Inorg. Chem.* **1992**, *13*, 359.
(2) Rossenaar, B. D.; Kleverlaan, C. J.; Stufkens, D. J.; Oskam, A. *J. Chem. Soc., Chem. Commun.* **1994**, 63.
(3) Rossenaar, B. D.; Kleverlaan, C. J.; van de Ven, M. C. E.; Stufkens, D. J.; Vlcek, A., Jr. *Chem. Eur. J.* **1996**, *2*, 228.
(4) Rossenaar, B. D.; George, M. W.; Johnson, F. P. A.; Stufkens, D. J.; Turner, J. J.; Vlcek, A., Jr. *J. Am. Chem. Soc.* **1995**, *117*, 11582.
(5) Stufkens, D. J.; Aarnts, M. P.; Rossenaar, B. D.; Vlcek, A., Jr. *Pure Appl. Chem.* **1997**, *69*, 831.
(6) Stufkens, D. J.; Vlcek, A., Jr. *Coord. Chem. Rev.* **1998**, *177*, *127*.
(7) Rossenaar, B. D.; Lindsay, E.; Stufkens, D. J.; Vlcek, A., Jr. *Inorg. Chim. Acta* **1996**, *250*, 5.
(8) Rossenaar, B. D.; Stufkens, D. J.; Oskam, A.; Fraanje, J.; Goubitz, K. *Inorg. Chim. Acta* **1996**, *247*, 215.
(9) Kleverlaan, C. J.; Martino, D. M.; van Willigen, H.; Stufkens, D. J.; Oskam, A. *J. Phys. Chem.* **1996**, *100*, 18607.
(10) Kleverlaan, C. J.; Stufkens, D. J.; Clark, I. P.; George, M. W.; Turner, J. J.; Martino, D. M.; van Willigen, H.; Vlcek, A., Jr. *J. Am. Chem. Soc.* **1998**, *120*, 10871.
(11) Kleverlaan, C. J.; Stufkens, D. J. *Inorg. Chim. Acta* **1999**, *284*, 61.
(12) Aarnts, M. P.; Stufkens, D. J.; Wilms, M. P.; Baerends, E. J.; Vlcek, A., Jr.; Clark, I. P.; George, M. W.; Turner, J. J. *Chem. Eur. J.* **1996**, *2*, 1556.
(13) Aarnts, M. P.; Wilms, M. P.; Peelen, K.; Fraanje, J.; Goubitz, K.; Hartl, F.; Stufkens, D. J.; Baerends, E. J.; Vlcek, A., Jr. *Inorg. Chem.* **1996**, *35*, 5468.
(14) Aarnts, M. P.; Wilms, M. P.; Stufkens, D. J.; Baerends, E. J.; Vlcek, A., Jr. *Organometallics* **1997**, 16, 2055.
(15) Finger, K.; Daniel, C. *J. Chem. Soc., Chem. Commun.* **1995**, 63. Finger, K.; Daniel, C. *J. Am. Chem. Soc.* **1995**, *117*, 12322.
(16) Guillaumont, D.; Finger, K.; Hachey, M. R.; Daniel, C. *Coord. Chem. Rev.* **1998**, *171*, 439.
(17) Guillaumont, D.; Daniel, C. *Coord. Chem. Rev.* **1998**, 181, *177*.
(18) Guillaumont, D.; Wilms, M. P.; Daniel, C.; Stufkens, D. J. *Inorg. Chem.* **1998**, *37*, 5816.

10.1021/ja992069g CCC: $18.00
Published on Web 12/02/1999

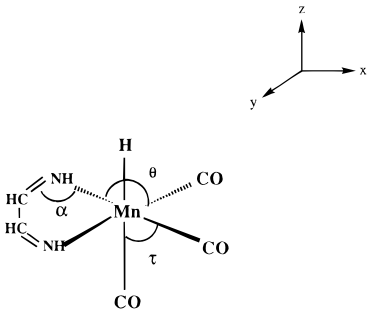

Figure 1. Idealized structure of $Mn(H)(CO)_3$(H-DAB).

molecules. An increase of the delocalization of the electronic density through these three centers modifies fundamentally the character of the low-lying excited states from purely metal-to-ligand charge-transfer (MLCT) to mixed MLCT/σ-bond-to-ligand charge-transfer (SBLCT).

We present here a complete quantum chemical study of the photodissociation dynamics of the title molecule in order to propose a semiquantitative deactivation mechanism of the molecule after visible and UV irradiation. This numerical simulation is based on the two-dimensional potential energy surfaces (PES) calculated for the electronic ground state and the lowest excited states as a function of the Mn−H and Mn−CO_{ax} bonds elongations.The excited states dynamics are investigated through wave packet propagations on these PES.

II. Computational Method

Quantum Chemical Calculations. The calculations were carried out under the C_s symmetry constraint starting from an idealized geometry as depicted in Figure 1 for the a^1A' electronic ground state corresponding to the $(\sigma_{Mn-H})^2(3d_{x^2-y^2})^2(3d_{yz})^2(3d_{xz})^2$ electronic configuration and for the low-lying $^{1,3}A'$ and $^{1,3}A''$ MLCT, SBLCT, and metal-centered (MC) excited states corresponding to $3d \rightarrow \pi^*_{H-DAB}$, $\sigma_{Mn-H} \rightarrow \pi^*_{H-DAB}$, and $3d \rightarrow 3d$ excitations, respectively. Idealized geometries were deduced from the ground-state structures of $MnCl(CO)_3$(Ph-DAB) (Ph = phenyl)[19] and of $HMn(CO)_5$[20] with the following bond lengths: Mn−H = 1.576 Å, Mn−CO_{ax} = 1.820 Å, Mn−CO_{eq} = 1.807 Å, Mn−N = 2.032 Å, N−C = 1.280 Å, C−C = 1.508 Å, N−H = 1.010 Å, C−H = 1.080 Å. The angles τ, θ, and α were kept constant at 90°, 96°, and 117,5°, respectively.

Gradient/CASSCF optimizations have been performed for the electronic ground state and a few excited states: the lowest a^3A' MLCT state corresponding to the $3d_{xz} \rightarrow \pi^*_{H-DAB}$ excitation, the c^3A' SBLCT state corresponding to the $\sigma_{Mn-H} \rightarrow \pi^*_{H-DAB}$ excitation, and the b^1A' MLCT state corresponding to the $3d_{x^2-y^2} \rightarrow \pi^*_{H-DAB}$ excitation. The study of the molecule deformation when going from the electronic ground state to the excited states was the purpose of these calculations. The electronic states and the two-dimensional PES $V(q_a,q_b)$, with q_a = [Mn−H] and q_b = [Mn−CO_{ax}], keeping the C_s symmetry constraint (Scheme 1) (see Results section for the choice of coordinates), have been obtained through complete active space SCF (CASSCF) calculations supplemented by a multireference contracted configuration interaction MR-CCI treatment. For each electronic state 30−35 ab initio points have been computed, and the whole potentials have been fitted numerically on the basis of the bicubic spline procedure.

Since our interest centers mostly on excited states of $Mn(H)(CO)_3$-(H-DAB) corresponding to $3d \rightarrow \pi^*_{H-DAB}$, $\sigma_{Mn-H} \rightarrow \pi^*_{H-DAB}$, and $3d \rightarrow 3d$ excitations in the principal configuration, the CASSCF active space is limited to the 3d occupied orbitals of Mn and the 3d orbitals which correlate them, the vacant 3d orbital, the bonding σ_{Mn-H} and antibonding σ^*_{Mn-H} orbitals involved in the Mn−H bond, and the low-lying π^*_{H-DAB} orbital. Eight electrons were correlated in 10 active orbitals in these so-called 8e10a CASSCF calculations averaged over five roots of a given spin and a given symmetry ($^{1,3}A'$ and $^{1,3}A''$). For each electronic state multireference CCI calculations have been carried out, including all the configurations that appear with coefficients larger than 0.08 in the CASSCF expansion correlating eight electrons and including single and double excitations to all virtuals orbitals, except the counterparts of the carbonyls 1s and the metal 1s, 2s, and 2p. The following ANO basis sets were used:[21] for the metal center a (17s,12p,9d) set contracted to [6s,4p,3d], for the second-row atoms a (10s,6p,3d) set contracted to [3s,2p], for the hydrogen linked to the metal center a (7s,3p) set contracted to [3s,1p], and for the other hydrogen atoms a (7s,3p) set contracted to [2s]. CASPT2 excitation energies have been calculated for the a^3A' and b^3A' excited states, based on the averaged CASSCF wave function used for the MR-CCI calculations. However, our attempt at performing reference CASPT2 calculations for the other states has failed either because of their less pure character, characterized by a large mixing of configurations at the CASSCF level, or because of the occurrence of intruder states. The 1s, 2s, and 2p electrons of the Mn atom and the 1s electrons of the second-row atoms have been frozen in the CASPT2 calculations.

The CASSCF/MR-CCI calculations have been performed with the MOLCAS-3 Quantum Chemistry software.[22] The geometry optimizations have been carried out either with MOLCAS-3 or with HONDO.[23] The electronic diopole transition moments have been estimated at the CASSCF level. The spin−orbit coupling between the singlet and the triplet states has been evaluated using a restricted full CI scheme and an effective one-electron SO operator, operating on the metal center in the L−S coupling scheme.[24] Since only the first derivative part of the kinetic coupling is needed in our approach of the nonadiabatic effects, the kinetic coupling around avoided crossings has been approximated by Lorentzians in order to avoid fastidious numerical differentiation of the electronic CASSCF wave functions.[25]

Simulation of the Dynamics. For the sake of simplicity the molecule is modeled as pseudotriatomic with two collinear dissociative bonds q_a = [Mn−H] and q_b = [Mn−CO_{ax}] (Scheme 1). These two coordinates are the most significantly affected on going from the electronic ground state to the excited states and conserve the C_s symmetry. All other "spectator" modes are decoupled in this zero-order approximation. This approximation should be reasonable, at least for ultrafast time scales (<1 ps) when energy remains in the dissociative bond.

The photoabsorption and the photodissociation dynamics are simulated by propagation of selected wave packets $\Psi_k(q_a,q_b,t)$ on the potentials $V^d_k(q_a,q_b)$ corresponding to the electronic states k. The time evolution of the wave packet is obtained by solving a set of coupled time-dependent Schrödinger equations in the diabatic representation

$$i\hbar\frac{\partial}{\partial t}\Psi_k(q_a,q_b,t) = [T_{nu} + V^d_k]\Psi_k(q_a,q_b,t) + \sum_{k \neq k'} V^d_{kk'}\Psi_{k'}(q_a,q_b,t) \quad (1)$$

with the following initial conditions

$$\Psi_k(q_a,q_b,t=0) = \mu_k\Phi_{gs,0,0}(q_a,q_b) \quad (2)$$

where μ_k is the electronic transition dipole moment between the electronic ground state (gs) and the electronic excited-state k. $\Phi_{gs,0,0}$-(q_a,q_b) represents the two-dimensional vibrational ground-state wave function of the electronic ground-state evaluated through the coupled Morse oscillators method.[26] In the case of preliminary one-dimensional

(19) Schmidt, G. S.; Paulus, H.; van Eldik, R.; Elias, H. *Inorg. Chem.* **1988**, *27*, 3211.

(20) McNeill, E. A.; Schöler, F. R. *J. Am. Chem. Soc.* **1977**, *99*, 6243.

(21) Pierlot, K.; Dumez, B.; Widmark, P. O.; Roos, B. O. *Theor. Chim. Acta* **1995**, *90*, 87.

(22) Andersson, K.; Blomberg, M. R. A.; Fülscher, M. P.; Karlström, G.; Kellö, V.; Lindh, R.; Malmqvist, P.-Å.; Noga, J.; Olsen, J.; Roos, B. O.; Sadlej, A. J.; Siegbahn, P. E. M.; Urban, M.; Widmark, P.-O. Molcas-3.0, University of Lund, Sweden. The MR-CCI program is based on the original program developed by Siegbahn: Siegbahn, P. E. M. *Int. J. Quantum Chem.* **1983**, *23*, 1869.

(23) Dupuis, M.; Johnston, F.; Marquez, A. Hondo-8.5, IBM Corp., Kingston, NY, 12401.

(24) Ribbing, C.; Daniel, C. *J. Chem. Phys.* **1994**, *100*, 6591.

(25) Finger, K.; Daniel, C.; Saalfrank, P.; Schmidt, B. *J. Phys. Chem.* **1996**, *100*, 3368.

(26) Hartke, B.; Manz, J.; Mathis, J. *Chem. Phys.* **1989**, *139*, 123. Joseph, T.; Kruel, T. M.; Manz, J.; Rexrodt, I. *Chem. Phys.* **1989**, *139*, 323.

Scheme 1

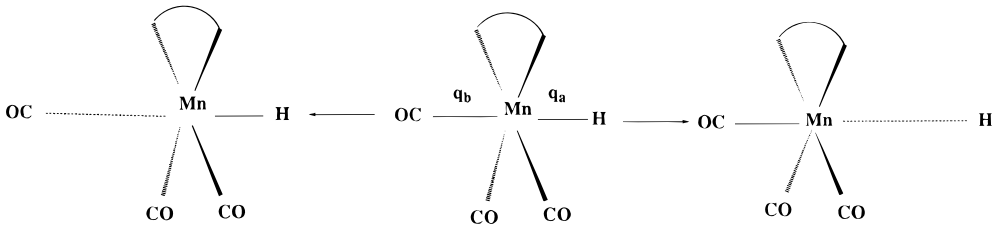

simulations, along one of the coordinates q_a or q_b, the eigenstates of the electronic ground state are calculated through the Fourier grid Hamiltonian method.[27]

The potential couplings $V^d_{kk'}$ are given either by the spin−orbit coupling elements of the SOC-CI matrix (singlet−triplet interactions) or by the transformation of the estimated kinetic couplings around avoided crossings (singlet−singlet and triplet−triplet interactions). The adiabatic/diabatic transformation is performed according to the scheme proposed in ref 25.

The solution of the time-dependent Schrödinger equation (eq 1) is obtained either by the second-order-differential (SOD) propagation scheme[28] with $\Delta t = 7.26 \times 10^{-3}$ fs or by the Chebychev propagation scheme[29] with $\Delta t = 10$ fs. The propagations are based on representations of $\Psi_k(q_a,q_b,t)$ on two-dimensional grids with the following parameters: $q_a i = q_{a_0} + (i-1)\Delta q_a$, $q_{a_0} = 2.2677$ au, $\Delta q_a = 0.11$ au with $1 \le i \le 128$; and $q_b j = q_{b0} + (j-1)\Delta q_b$, $q_{b0} = 2.6456$ au, $\Delta q_b = 0.0057$ au with $i \le j \le 128$.

The absorption spectrum σ_{tot} is obtained by the Fourier transform of the total autocorrelation function $S_{tot}(t)$ summed over the individual autocorrelation functions corresponding to each excited-state k,

$$\sigma_{tot}(\omega) \propto \omega \int_{-\infty}^{+\infty} dt\, e^{i(Ei+\omega)t} S_{tot}(t) \tag{3}$$

where

$$S_{tot}(t) = \sum_k \langle \Psi_k(0) | \Psi_k(t) \rangle \tag{4}$$

and E_i represents the energy of the initial wave packet on the electronic state k.

The kinetic part of the Hamiltonian of the system, expressed in bond coordinates, is given by

$$T_{nu} = -\frac{\hbar^2}{2\mu_a}\frac{\partial^2}{\partial q_a^2} - \frac{\hbar^2}{2\mu_b}\frac{\partial^2}{\partial q_b^2} + \frac{\hbar^2}{m_c}\frac{\partial^2}{\partial q_a \partial q_b} \tag{5}$$

where μ_a and μ_b are the reduced masses corresponding to the bonds q_a and q_b and m_c is the mass of the central atom. Reaction probabilities are deduced by integration, over the whole reaction time, of the probability current density expressed as a function of coordinates q_a and q_b[30] (with $\theta = 180°$).

$$\vec{J}(q_a,q_b,t) = \begin{pmatrix} J_a(q_a,q_b,t) \\ J_b(q_a,q_b,t) \end{pmatrix} \tag{6}$$

where

$$J_b(q_a,q_b,t) = \frac{1}{\mu_a} Re\left(\Psi^*(q_a,q_b,t) \frac{\hbar}{i} \frac{\partial}{\partial q_a} \Psi(q_a,q_b,t) \right) + \frac{\cos\vartheta}{m_c} Re\left(\Psi^*(q_a,q_b,t) \frac{\hbar}{i} \frac{\partial}{\partial q_b} \Psi(q_a,q_b,t) \right) \tag{7}$$

and $J_b(q_a,q_b,t)$ being defined in a symmetric way.

In the case of prelimimary one-dimensional simulations (along either q_a = [Mn−H] or q_b = [Mn−CO$_{ax}$] coordinates) the dissociation probability is simply given by the following expression:

$$P_{diss}(t) = 1 - \sum_k \int_{q_0}^{q_{diss}} |\Psi_k(q,t)|^2\, dq \tag{8}$$

where q_0 and q_{diss} represent the lower and dissociation limits of the grid, respectively.

III. Results and Discussion

Geometrical Structures. The method of optimization has been tested on HMn(CO)$_5$ in its electronic ground state for which the experimental structure is known.[20] The agreement between the optimized bond lengths and bond angles and the experimental values is rather good[31] and very similar to the one reported in other studies of first-row transition metal carbonyls,[32−34] namely a maximum of error for the Mn−CO$_{eq}$ bond distance overestimated by 4%. Taking into account dynamical correlation effects in a post-CASSCF treatment should improve our results. Our purpose in the context of the present work being to infer the main qualitative trends when exciting the molecule, no further investigations of these correlation effects have been undertaken.

To evaluate the structural deformations when going from the a^1A' electronic ground state to the low-lying MLCT and SBLCT states, tentative geometry optimizations have been performed at the CASSCF level (8e10a) under the C_s symmetry constraint. The optimized structures of the lowest a^3A' MLCT state corresponding to the $3d_{xz} \rightarrow \pi^*_{H-DAB}$ excitation, the c^3A' SBLCT state corresponding to the $\sigma_{Mn-H} \rightarrow \pi^*_{H-DAB}$ excitation, and the b^1A' MLCT state corresponding to the $3d_{x^2-y^2} \rightarrow \pi^*_{H-DAB}$ excitation are reported in Table 1. Optimization of other electronic states has failed because of convergence problems at the CASSCF level. In particular, it has not been possible to optimize the structure of the molecule in the c^1A' MLCT state corresponding to the $3d_{xz} \rightarrow \pi^*_{H-DAB}$ excitation which contributes mainly to the absorption spectrum.

The main structural deformations of Mn(H)(CO)$_3$(H-DAB) after excitation to these low-lying states are represented in Figure 2. According to our preliminary investigations[31] the flexibility of the molecule when going from the electronic ground state to the low-lying excited states either of MLCT type or of SBLCT type is poor. The small deformation of the molecule in the MLCT states is corroborated by the presence of an intense emission at 500 nm matching perfectly with the absorption band and typical of a number of MLCT complexes of this class.[35] The angular deformations never exceed 10%, and the only bond length elongations which exceed 10% are the Mn−CO$_{ax}$ bond

(27) Marston, C. C.; Balint-Kurti, G. G. *J. Chem. Phys*. **1989**, *91*, 3571.
(28) Askar, A.; Cakmak, A. S. *J. Chem. Phys*. **1978**, *68*, 2794.
(29) Tal-Ezer, H.; Kosloff, R. *J. Chem. Phys*. **1984**, *81*, 3967.
(30) Katz, G.; Baer, R.; Kosloff, R. *Chem. Phys. Lett*. **1995**, *239*, 230.
(31) Guillaumont, D.; Daniel, C. *Chem. Phys. Lett*. **1996**, *257*, 1.
(32) Persson, B. J.; Roos, B. O.; Pierloot, K. *J. Chem. Phys*. **1994**, *101*, 6810.
(33) Ziegler, T.; Tschinke, V.; Ursenbach, C. *J. Am. Chem. Soc*. **1987**, *109*, 4825.
(34) Ehlers, W. A.; Frenking, G. *Organometallics* **1995**, *14*, *423*.
(35) Kleverlaan, C. J. Ph.D. Thesis, University of Amsterdam, The Netherlands, 1998. Rossenaar, B. D. Ph.D. Thesis, University of Amsterdam, The Netherlands, 1995.

Table 1. CASSCF Optimized Bond Lengths (in Å) and Bond Angles (in Degrees) in the a^1A' Electronic Ground State and the a^3A' and b^1A' MLCT and d^3A' SBLCT Excited States

	idealized geometry	a^1A' electronic ground state[a]	a^3A' $3d_{xz} \rightarrow \pi^*_{H-DAB}$ MLCT	b^1A' $3d_{x^2-y^2} \rightarrow \pi^*_{HDAB}$ MLCT	d^3A' $\sigma_{Mn-H} \rightarrow \pi^*_{H-DAB}$ SBLCT
			Bond Lengths		
Mn−H	1.576	1.617 (1.625)	1.578	1.571	1.946
$Mn-C_{ax}$	1.820	1.902 (1.918)	2.172	2.018	2.040
$Mn-C_{eq}$	1.807	1.885 (1.893)	1.918	1.979	1.941
Mn−N	2.032	2.068 (2.072)	2.073	2.069	2.090
C−O	1.142	1.160 (1.151)	1.154	1.148	1.145
N−C	1.280	1.288 (1.285)	1.338	1.339	1.338
C−C	1.508	1.465 (1.463)	1.417	1.413	1.409
			Bond Angles		
$HMnC_{eq}$	90.0	81.2 (80.6)	77.3	82.4	91.4
HMnN	90.0	87.2 (87.4)	98.2	86.5	81.2
$HMnC_{ax}$	180.0	174.5 (177.6)	167.2	174.1	169.4
$NMnC_{ax}$	90.0	97.2 (94.7)	91.7	89.0	90.6
NMnN	78.0	73.3 (75.7)	78.1	79.4	78.5
NCC	114.2	114.3 (115.5)	116.6	117.4	117.5
$C_{eq}MnC_{eq}$	90.0	94.1 (92.9)	101.5	93.7	96.3
$NMnC_{eq}$	96.0	94.1 (94.5)	89.8	92.3	92.2
MnNC	117.5	118.1 (116.6)	114.2	112.5	113.2

[a] Values in parentheses have been obtained through 8e9a CASSCF calculations of ref 31.

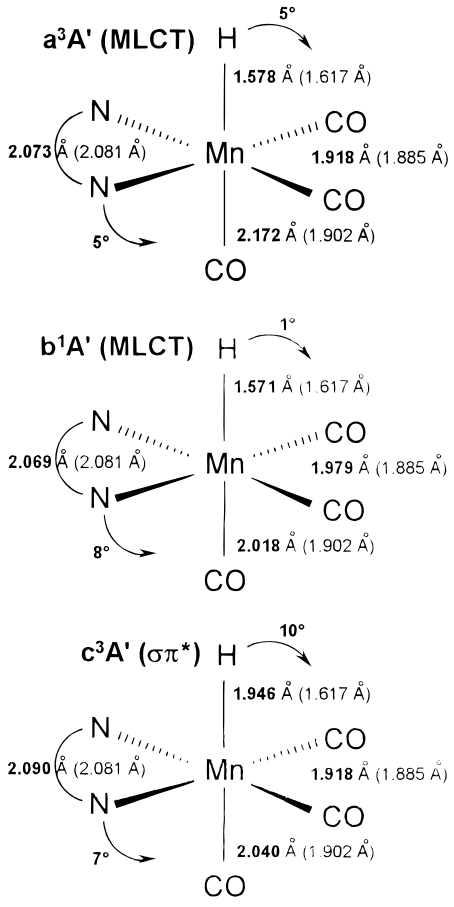

Figure 2. CASSCF/MR-CCI optimized geometries of the a^3A', c^3A', and b^1A' electronic excited states of $Mn(H)(CO)_3$(H-DAB) as compared to the electronic ground-state optimized geometry (values in parentheses). The angular deformations are given near the arcs.

in the ^{3}MLCT ($3d_{xz} \rightarrow \pi^*_{H-DAB}$) state and the Mn−H bond in the ^{3}SBLCT ($\sigma_{Mn-H} \rightarrow \pi^*_{H-DAB}$), which increase by 14% and 20%, respectively.

Most of the bond lengths are only slightly modified (<5%). It is worth noting that, whereas the Mn−H bond length increases in the ^{3}SBLCT state, it decreases by 4% and 3% in the ^{3}MLCT and ^{1}MLCT states, respectively. These trends point to a dissociative character of the ^{3}SBLCT state for the metal−hydrogen bond homolysis and to a quasi-bound nature of the MLCT states for this reaction.[15] On the basis of these results, the theoretical study has been restricted to the two coordinates q_a = [Mn−H] and q_b = [Mn−CO_{ax}], the rest of the molecule being frozen to the ground-state geometry. This is justified by the goal of the present work having to do with vertical transitions in the Franck−Condon domain followed by ultrafast dissociative processes occurring in femtosecond to picosecond time scales which are not competitive with vibrational relaxations. Moreover, a recent time-resolved spectroscopic study of $[Ru(bpy)_3]^{2+}$ has shown that the absorption spectrum is resolved in less than 200 fs.[36] Clearly, the investigation of other photophysical properties connected to long-lived excited states (e.g., emission spectra) should take into account the relaxation effects neglected in this study.

Table 2. CASSCF/MR-CCI Excitation Energies (in cm^{-1}) to the Low-Lying $^1A'$ and $^1A''$ Excited States of $Mn(H)(CO)_3$(H-DAB) and Corresponding Oscillator Strengths *f*

transition	one-electron excitation in the principal configuration	CASSCF/ MR-CCI[a]	f
$a^1A' \rightarrow a^1A''$	$3d_{yz} \rightarrow \pi^*_{H-DAB}$	18 000	0.04
$a^1A' \rightarrow b^1A'$	$3d_{x^2-y^2} \rightarrow \pi^*_{H-DAB}$	21 060	0.03
$a^1A' \rightarrow c^1A'$	$3d_{xz} \rightarrow \pi^*_{H-DAB}$	23 020	0.39
$a^1A' \rightarrow b^1A''$	$3d_{x^2-y^2} \rightarrow 3d_{xy}$	29 000	0.01
$a^1A' \rightarrow c^1A''$	$3d_{xz} \rightarrow 3d_{xy}$	34 000	0.00
$a^1A' \rightarrow d^1A'$	$3d_{yz} \rightarrow 3d_{xy}$	33 400	0.02
$a^1A' \rightarrow e^1A'$	$\sigma_{Mn-H} \rightarrow \pi^*_{H-DAB}$	35 600	0.11

Theoretical Absorption Spectrum. The CASSCF/MR-CCI excitation energies to the low-lying singlet and triplet excited states of $Mn(H)(CO)_3$(H-DAB) are collected in Tables 2 and 3, respectively.

The visible part of the absorption spectrum consists of three MLCT states corresponding to $3d \rightarrow \pi^*_{H-DAB}$ excitations and ranging between 18 000 and 23 020 cm^{-1}. The c^1A' ($3d_{xz} \rightarrow \pi^*_{H-DAB}$) state is the only one which has a sufficient oscillator strength (f = 0.39) to contribute significantly to the visible absorption. The UV absorption is composed of three MC states corresponding to $3d \rightarrow 3d$ excitations calculated between 29 000 and 33 400 cm^{-1} with very low oscillator strengths (≤0.02) and

(36) McCusker, J. K. 12th ISPPCC, Colchester, VT, 1997.

Table 3. CASSCF/MR-CCI Excitation Energies (in cm^{-1}) to the Low-Lying ^{3}A′ and ^{3}A″ Excited States of Mn(H)(CO)$_3$(H-DAB)

transition	one-electron excitation in the principal configuration	CASSCF/ MR-CCI[a]	CASPT2
a^{1}A′ → a^{3}A′	$3d_{xz} \rightarrow \pi^*_{H-DAB}$	16 100	16 300
a^{1}A′ → a^{3}A″	$3d_{yz} \rightarrow \pi^*_{H-DAB}$	17 200	
a^{1}A′ → b^{3}A′	$3d_{x^2-y^2} \rightarrow \pi^*_{H-DAB}$	19 200	19 000
a^{1}A′ → c^{3}A′	$3d_{yz} \rightarrow 3d_{xy}$	26 400	
a^{1}A′ → d^{3}A′	$\sigma_{Mn-H} \rightarrow \pi^*_{H-DAB}$	34 400	

of one SBLCT state corresponding to the $\sigma_{Mn-H} \rightarrow \pi^*_{H-DAB}$ excitation calculated at 35 600 cm^{-1} with an oscillator strength of 0.11. The calculation of the triplet states has been restricted to the few states which may participate in the early photochemistry, namely the low-lying MLCT states (a^{3}A′, a^{3}A″, b^{3}A′), the ^{3}SBLCT (d^{3}A′) state which is dissociative for the Mn−H bond,[15] and the c^{3}A′ MC state. The CASSCF/MR-CCI excitation energies agree perfectly with the CASPT2 values (Table 3) obtained for the a^{3}A′ and b^{3}A′ MLCT states for which it has been possible to avoid serious intruder state problems. The singlet−triplet energy gap (<2000 cm^{-1}) is small for the excited states delocalized on the π^*_{H-DAB} acceptor ligand (MLCT or SBLCT), whereas it becomes significantly large (>5000 cm^{-1}) for the MC state. The particular behavior of the MLCT state corresponding to the $3d_{xz} \rightarrow \pi^*_{H-DAB}$ is due to an important interaction between its singlet component with the electronic ground state illustrated by a low CI coefficient on the principal configuration of 0.75 for the c^{1}A′ state vs a value of the order of 0.85 for the other MLCT states. This interaction explains the unusually large singlet−triplet energy gap (7000 cm^{-1}) for this MLCT state which is a consequence of the singlet component destabilization. The character of the low-lying excited states of Mn(H)(CO)$_3$(H-DAB) in the Franck−Condon region is nearly pure, either MLCT, SBLCT, or MC.

The SOC terms between the low-lying triplet and singlet states are reported in Table 4. SOC values have been evaluated through a restricted full-CI scheme[24] based on a unique CASSCF wave function optimized either for the triplet states or for the singlet states. In these calculations, limited to a small active space, it has not been possible to obtain the d^{1}A′ MC excited state which needs large CI expansions to be described properly. The corresponding SO splitting of the triplet states obtained after diagonalization of the SOC-CI matrix never exceeds 60 cm^{-1} and may be neglected. The SOC values range between 0 and 140 cm^{-1}. In a recent paper these interactions have been analyzed on the basis of the orientation of the orbitals involved in the electronic transition, and their effect on the Mn−H bond homolysis has been discussed.[37] For instance, it has been shown that the ^{1}SBLCT → a^{3}MLCT transition which is accompanied by the jump of one electron from the $3d_{xz}$ (*xz* oriented) to the σ_{Mn-H} orbital (*z* oriented) is more efficient than the ^{1}SBLCT → ^{3}SBLCT transition for which there is no such spin-flip possibility. This is illustrated by the relatively high value of SOC in the former case (100 cm^{-1}) compared to the latter one (0 cm^{-1}). The nearly pure nature of the excited states allows this qualitative analysis.

The theoretical spectrum obtained by propagation of the $\Psi_{b^1A'}(q_a,q_b,t)$, $\Psi_{c^1A'}(q_a,q_b,t)$, and $\Psi_{e^1A'}(q_a,q_b,t)$ wave packets on the corresponding b^{1}A′, c^{1}A′, and e^{1}A′ PES (the details of the simulation are described in the next sections) with the initial conditions given by eq 2,

$$\Psi_{b^1A'}(q_a,q_b,t=0) = 0.23\Phi_{a^1A',0,0}(q_a,q_b) \quad (9)$$

$$\Psi_{c^1A'}(q_a,q_b,t=0) = 2.22\Phi_{a^1A',0,0}(q_a,q_b) \quad (10)$$

$$\Psi_{e^1A'}(q_a,q_b,t=0) = 0.99\Phi_{a^1A',0,0}(q_a,q_b) \quad (11)$$

is shown in Figure 3a.

Only the low-lying ^{1}A′ MLCT and ^{1}SBLCT states have been retained in this two-dimensional simulation. The d^{1}A′ (MC) state has been excluded since the achievement of the corresponding two-dimensional PES has failed due to convergence problems. The ^{1}A″ states have not been taken into account due to their low oscillator strengths (Table 2). The absorption spectrum (Figure 3a) exhibits an intense peak centered around 22 000 cm^{-1} (450 nm) and a shoulder centered around 35 000 cm^{-1} (285 nm). The vibronic structures (dashed lines) are obtained by the Fourier transform of the autocorrelation function $S_{tot}(t)$ (eq 4) and the envelope by multiplying the original autocorrelation function by an exponential term in order to take into account qualitatively the effect of an increasing number of degrees of freedom. It reproduces the main features of the experimental spectrum obtained for this class of molecules as illustrated in Figure 3b. Indeed, the UV−visible spectrum of Mn(Me)(CO)$_3$(^{i}Pr-DAB) measured at low temperature[38] shows a first intense band in the visible (E_{max} = 20 000 cm^{-1}) assigned to the a^{1}A′ → c^{1}A′ transition and a second less intense shoulder in the UV region (E_{max} = 30 000 cm^{-1}) assigned to the a^{1}A′→ d^{1}A′ and a^{1}A′ → e^{1}A′ transitions. The first band presents a negative solvatochromism typical of the MLCT states.[39]

Potential Energy Curves for the Homolytic Rupture of the Manganese−Hydrogen Bond. The MR-CCI energies for the a^{1}A′ electronic ground state and the low-lying singlet and triplet excited states of Mn(H)(CO)$_3$(H-DAB) of A′ symmetry, calculated along the Mn−H bond homolysis reaction path under the C_s symmetry constraint, are reported in Table 5. The corresponding adiabatic potential energy curves are shown in Figure 4a and 4b for the singlet and triplet states, respectively.

The reaction is calculated to be endothermic by 55.0 kcal mol^{-1} in agreement with the Mn−H bond energy in transition metal hydrides.[40] The formation of the diradical H$^\bullet$ + $^\bullet$Mn(CO)$_3$(H-DAB) primary products rests on the change of character of the a^{1}A′ potential as a function of q_a = [Mn−H]. At equilibrium (q_a = 1.576 Å) the a^{1}A′ is described by the following electronic configuration, $(\sigma_{Mn-H})^2(3d_{x^2-y^2})^2(3d_{yz})^2(3d_{xz})^2(\sigma^*_{Mn-H})^0$, where the σ_{Mn-H} and σ^*_{Mn-H} orbitals are bonding and antibonding combinations of the s_H orbitals with the $3d_{z^2} + \epsilon\pi^*_{H-DAB}$ and $3d_{z^2} - \epsilon\pi^*_{H-DAB}$, respectively. The π^*_{H-DAB} character of these latter orbitals increases as a function of the q_a coordinate, leading to $\pi^*_{H-DAB} + 3d_{z^2}$ and $3d_{z^2} - \pi^*_{H-DAB}$ combinations at the asymptote. At dissociation, the electronic configuration of the a^{1}A′ state is given by $(s_H)^0(3d_{x^2-y^2})^2(3d_{yz})^2(3d_{xz})^2(\pi^*_{H-DAB} + 3d_{z^2})^2$ which is nearly degenerate (see Table 5) with the corresponding a^{3}A′ $(s_H)^1(3d_{x^2-y^2})^2(3d_{yz})^2(3d_{xz})^2(\pi^*_{H-DAB} + 3d_{z^2})^1$ describing the formation of the diradical. The low-lying MLCT states, namely b^{1}A′ and c^{1}A′, are bound and generate an avoided crossing around 2.6 Å. The mixing of the d^{1}A′ and e^{1}A′ excited states in the UV energy domain leads to a double-well potential in the Franck−Condon region. The singlet states are bound along the q_a coordinate and should not lead to fast direct homolytic cleavage of the Mn−H bond after visible absorption into the MLCT states.

(37) Daniel, C.; Guillaumont, D.; Ribbing, C.; Minaev, B. *J. Phys. Chem.* **1999**, *A103*, 5766.

(38) Guillaumont, D.; Aarnts, M.; Stufkens, D. J., unpublished work.

(39) Chen, P.; Meyer, T. J. *Chem. Rev.* **1998**, *98*, 1439. Hush, N. S.; Reimers, J. R. *Coord. Chem. Rev.* **1998**, *177*, 37.

(40) Kristjansdottir, S. S.; Norton, J. R. In *Transition Metal Hydrides*; Dedieu, A., Ed; VCH Publishers: New York, 1991; pp 309−359.

Table 4. Calculated Spin−Orbit Interactions (in cm^{-1}) in $Mn(H)(CO)_3$(H-DAB) at the CASSCF/SOC-CI Level ($Z_{eff} = 15.0$)[a]

	a^3A' $3d_{xz} \rightarrow \pi^*_{H-DAB}$ MLCT	b^3A' $3d_{x^2-y^2} \rightarrow \pi^*_{HDAB}$ MLCT	a^3A'' $3d_{yz} \rightarrow \pi^*_{H-DAB}$ MLCT	c^3A' $3d_{yz} \rightarrow 3d_{xy}$ MC	d^3A' $\sigma_{Mn-H} \rightarrow \pi^*_{H-DAB}$ SBLCT
a^1A' electronic ground state	20	60	40	140	70
b^1A' $3d_{x^2-y^2} \rightarrow \pi^*_{HDAB}$ MLCT	80	20	100	3	20
c^1A' $3d_{xz} \rightarrow \pi^*_{H-DAB}$ MLCT	45	60	2	9	75
e^1A' $\sigma_{Mn-H} \rightarrow \pi^*_{H-DAB}$ SBLCT	100	8	90	0	0

[a] From this work and ref 37.

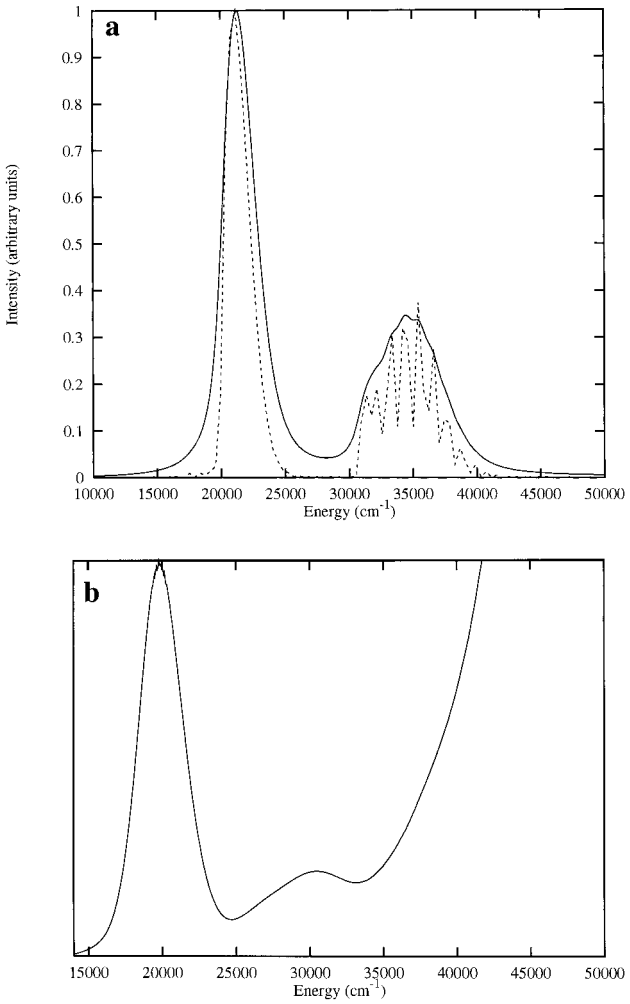

Figure 3. (a) Theoretical absorption spectrum of $Mn(H)(CO)_3$(H-DAB) (dashed line, vibronic structure obtained by Fourier transform of the autocorrelation function eq 4; continuous line, envelope obtained after multiplication of the original autocorrelation function by an exponential factor $\exp(-\Gamma t)$, $\Gamma = 0.13$). (b) Experimental absorption spectrum of $Mn(Me)(CO)_3$(^{i}Pr-DAB) measured at 183 K in a solution of dimethyl-2,2-butane/*n*-pentane (8:3).[38]

The shape of the triplet potentials (Figure 4b) indicates the presence of three low-lying bound states, namely the a^3A' and b^3A' MLCT states and the c^3A' MC state. The d^3A' state corresponding to the $\sigma_{Mn-H} \rightarrow \pi^*_{H-DAB}$ excitation is dissociative and generates several avoided crossings at 1.9, 2.1, and 2.2 Å with the c^3A', b^3A', and a^3A' states, respectively. Consequently, the a^3A' state is predissociative with an energy barrier of 21.0 kcal mol^{-1} along the reaction pathway. According to this qualitative picture, efficient indirect homolytic cleavage of the Mn−H bond after intersystem crossing via the low-lying triplet states is unlikely.

Potential Energy Curves for the Axial Carbonyl Loss. The MR-CCI energies for the a^1A' electronic ground state and the low-lying singlet and triplet excited states of $Mn(H)(CO)_3$(H-DAB) of A' symmetry, calculated along the $Mn-CO_{ax}$ bond dissociation pathway under the C_s symmetry constraint, are reported in Table 6.

The corresponding adiabatic potential energy curves are shown in Figure 5a and 5b for the singlet and triplet states, respectively. The reaction is calculated to be endothermic by 25.3 kcal mol^{-1}. This value is in the range (slightly below due to the presence of the π acceptor ligand) of the calculated values and experimental data available for the metal−carbonyl bond dissociation energy in transition metal carbonyls.[41]

The low-lying singlet and triplet MLCT states (b^1A', c^1A', a^3A', and b^3A') are nearly dissociative along this reaction path, in agreement with the elongation of the $Mn-CO_{ax}$ bond calculated in the ^{3}MLCT state (see Geometrical Structures section, above). This dissociative character associated with a weakening of the metal−carbonyl bond is due to a decrease of the $d\pi-p\pi$ back-donation between the metal and the axial carbonyl ligand when going from the electronic ground state to the MLCT states. The MC (d^1A') and SBLCT (e^1A') excited states generate an avoided crossing around 2.2 Å leading to a double-well potential. The triplet and singlet components of these two states are bound for this reaction pathway, especially the d^3A' state corresponding to the $\sigma_{Mn-H} \rightarrow \pi^*_{H-DAB}$ excitation which is dissociative for the concurrent reaction, namely the Mn−H bond homolysis. According to the shape of the potential energy curves, the axial CO loss should be a fast and efficient process after visible irradiation of $Mn(H)(CO)_3$(H-DAB).

Potential Energy Surfaces and Spin−Orbit Evolution. The two-dimensional CASSCF/MR-CCI potential energy surfaces calculated as a function of $q_a = [Mn-H]$ and $q_b = [Mn-CO_{ax}]$ reaction coordinates under the C_s symmetry constraint (see Scheme 1) are represented in Figure 6a, 6b, and 6c for the b^1A' and c^1A' MLCT states and the e^1A' SBLCT state, respectively. The MLCT PES present dissociative valleys along the $Mn-CO_{ax}$ reaction coordinate and energy barriers in the direction of the Mn−H bond homolysis, whereas the e^1A' SBLCT PES is bound in both directions. On the basis of the calculated excited states (Tables 2 and 3) and associated PES the following qualitative mechanism is proposed: after direct absorption to the c^1A' MLCT state calculated at 23 020 cm^{-1} with an oscillator strength of 0.39, an efficient direct dissociation toward the axial CO loss CO + $Mn(H)(CO)_2$(H-DAB) primary products is proposed.

The photochemistry of the complex after absorption in the UV energy domain should be inefficient. The occurrence of the Mn−H bond homolysis in $Mn(H)(CO)_3$(H-DAB) will depend on the efficiency of the ^{1}MLCT → ^{3}SBLCT intersystem crossing.

To obtain a quantitative mechanism with information on the time scales and probabilities of the primary reactions, on the population of the different excited states after visible and UV irradiation, and on the efficiency of intersystem crossing

(41) See refs 15 and 34 and references therein.

Table 5. MR-CCI Energies Values (in au and Relative to −1675) of the Electronic Ground State (a^1A') and Low-Lying Excited States of Mn(H)(CO)$_3$(H-DAB) as a function of q_a = [Mn−H] (Mn−CO$_{ax}$ = 1.82 Å)

	Mn−H									
	1.4 Å	1.576 Å	1.8 Å	1.9 Å	2.0 Å	2.2 Å	2.5 Å	2.9 Å	3.5 Å	50.0 Å
a^1A'	0.25556	0.27161	0.26346	0.25568	0.24812	0.23208	0.21312	0.19010	0.17823	0.18413
b^1A'	0.16168	0.17567	0.16569	0.16187	0.15617	0.14474	0.13138	0.12385	0.11935	0.12862
c^1A'	0.14525	0.16672	0.14575	0.14272	0.13670	0.13358	0.12970	0.11167		0.12999
d^1A'	0.09823	0.11941	0.11058			0.12324	0.10777	0.08310	0.08821	0.08350
e^1A'		0.10940	0.09936	0.0859						
a^3A'	0.19387	0.19825	0.19438	0.18725	0.17799	0.16934	0.17423	0.17625	0.17688	0.18493
b^3A'	0.17367	0.18414	0.17447	0.16691	0.15035	0.14234	0.13133	0.12435	0.12308	0.13016
c^3A'	0.14488	0.15140	0.14631	0.13894	0.13990		0.12122	0.11436		
d^3A'	0.07673	0.11492	0.13352	0.13196	0.13123					

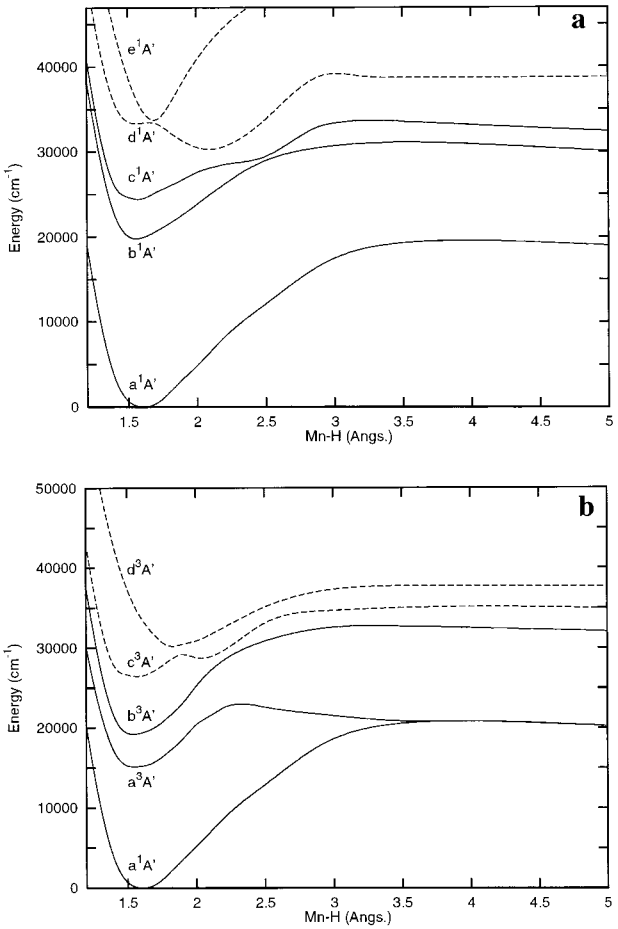

Figure 4. CASSCF/MR-CCI potential energy curves along q_a = [Mn−H] bond elongation in Mn(H)(CO)$_3$(H-DAB) for the low-lying singlet (a) and triplet (b) excited states.

processes, several one- and two-dimensional simulations of the excited states dynamics have been performed using wave packet propagations on spin−orbit and nonadiabatically coupled potentials.

The spin−orbit coupling values evaluated as a function of the reaction coordinates vary between 0 and 200 cm^{-1}. The fluctuations of the SO interactions reflect the change of character of the electronic states as a function of the reaction coordinates, especially along the Mn−H bond elongation, where several avoided crossings occur, between 2.0 and 2.5 Å. In the Franck−Condon region the triplet state is purely MLCT. When the metal−hydrogen bond is elongated the mixing between this state and the d^3A' (SBLCT) increases. Accordingly the c^1A'/a^3A' SOC increases (since the ^{3}MLCT state gains some SBLCT character) whereas the c^1A'/d^3A' SOC decreases (since the ^{3}SBLCT state gains some MLCT character).[37]

One-Dimensional Simulation on Spin−Orbit Coupled Potentials. To select the excited states playing a key role in the photodissociation mechanism and to determine the contribution of the triplet states, one-dimensional wave packet propagations either along the q_a = [Mn−H] reaction coordinate or along the q_b = [Mn−CO$_{ax}$] reaction coordinate have been performed on spin−orbit and nonadiabatically coupled potentials. Seven potentials have been included in the simulation of the dynamics after absorption in the visible: the a^1A' electronic ground state, the b^1A' and c^1A' MLCT states ranging in the absorption energy domain, and the four triplet states corresponding to the a^3A' and b^3A' (MLCT), c^3A' (MC), and d^3A' (SBLCT) states. Two potentials have been added in the simulation of the dynamics after UV absorption, namely the d^1A' (MC) and e^1A' (SBLCT) states ranging in the energy domain.

The initial conditions are the following for the simulation of the visible absorption to the low-lying MLCT states,

$$\Psi_{b^1A'}(q,t=0) = 0.23\Phi_{a^1A',0}(q) \quad (12)$$

$$\Psi_{c^1A'}(q,t=0) = 0.22\Phi_{a^1A',0}(q) \quad (13)$$

whereas only the electronic states contributing to the UV band are populated in the simulation of the UV absorption,

$$\Psi_{b^1A'}(q,t=0) = 0 \quad (14)$$

$$\Psi_{c^1A'}(q,t=0) = 0 \quad (15)$$

$$\Psi_{d^1A'}(q,t=0) = 0.47\Phi_{a^1A',0}(q) \quad (16)$$

$$\Psi_{e^1A'}(q,t=0) = 0.99\Phi_{a^1A',0}(q) \quad (17)$$

Investigation of the population of the different excited states after 1 ps of simulation (visible absorption) along the Mn−H bond homolysis reaction path (Figure 7) indicates a very stable situation where the system is trapped in the potential well of the c^1A' state. The population of the b^1A' state never exceeds 0.2% with a coupling term $V^{max}(b^1A'/c^1A')$ = 220 cm^{-1}. The modest population of the triplet states after 1 ps of simulation reflects the low efficiency of the intersystem crossing processes. The probability for observing the Mn−H bond homolysis represented in Figure 8 is nearly 0 in 1 ps.

From the wave packet propagations along the q_b = [Mn−CO$_{ax}$] reaction coordinate one may extract the axial CO loss probability which is represented in Figure 9 as a function of the time. The direct dissociation from the c^1A' (MLCT) state reaches 70% in 500 fs, pointing to a very efficient primary reaction after irradiation in the visible region.

The results of the one-dimensional (along q_a = [Mn−H]) simulation of the UV absorption and of the subsequent processes are depicted in Figures10 and 11, which represent the population

Table 6. MR-CCI Energies Values (in au and Relative to −1675) of the Electronic Ground State (a^1A') and Low-Lying Excited States of $Mn(H)(CO)_3$(H-DAB) as a Function of $q_b = [Mn-CO_{ax}]$ (Mn−H = 1.576 Å)

	Mn−CO_{ax}							
	1.6 Å	1.82 Å	2.0 Å	2.2 Å	2.5 Å	3.0 Å	3.5 Å	50.0 Å
a^1A'	0.22941	0.27161	0.27623	0.26712	0.25438	0.24158	0.23722	0.23127
b^1A'	0.13161	0.17567	0.20142	0.20344	0.20080	0.19785	0.19808	0.19530
c^1A'	0.10532	0.16672	0.18503	0.18799	0.18707	0.18431	0.18676	0.18539
d^1A'	0.05833	0.11941	0.12864	0.12456	0.12233	0.10299	0.10703	0.10609
e^1A'	0.05598	0.10940	0.12322	0.12266	0.10692			
a^3A'	0.14150	0.19825	0.22566	0.23190	0.23275	0.23310	0.23258	0.22893
b^3A'	0.13862	0.18414	0.20963	0.21353	0.21410	0.21462	0.21622	0.21355
c^3A'	0.09812	0.15140	0.18615	0.19261	0.19101		0.16321	
d^3A'	0.07120	0.11492	0.13662	0.13896	0.13683		0.12541	

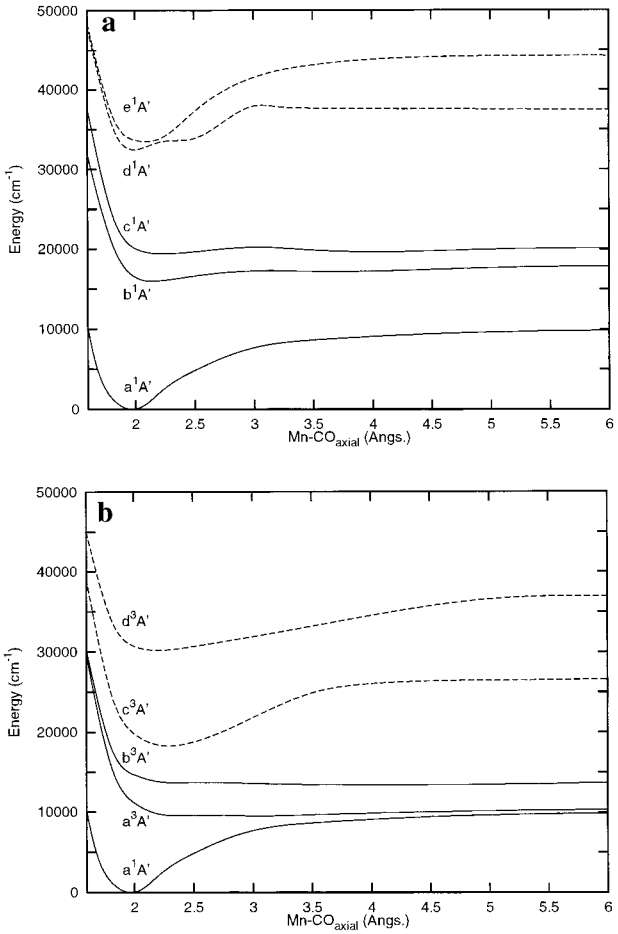

Figure 5. CASSCF/MR-CCI potential energy curves along $q_b = [Mn-CO_{ax}]$ bond elongation in $Mn(H)(CO)_3$(H-DAB) for the low-lying singlet (a) and triplet (b) excited states.

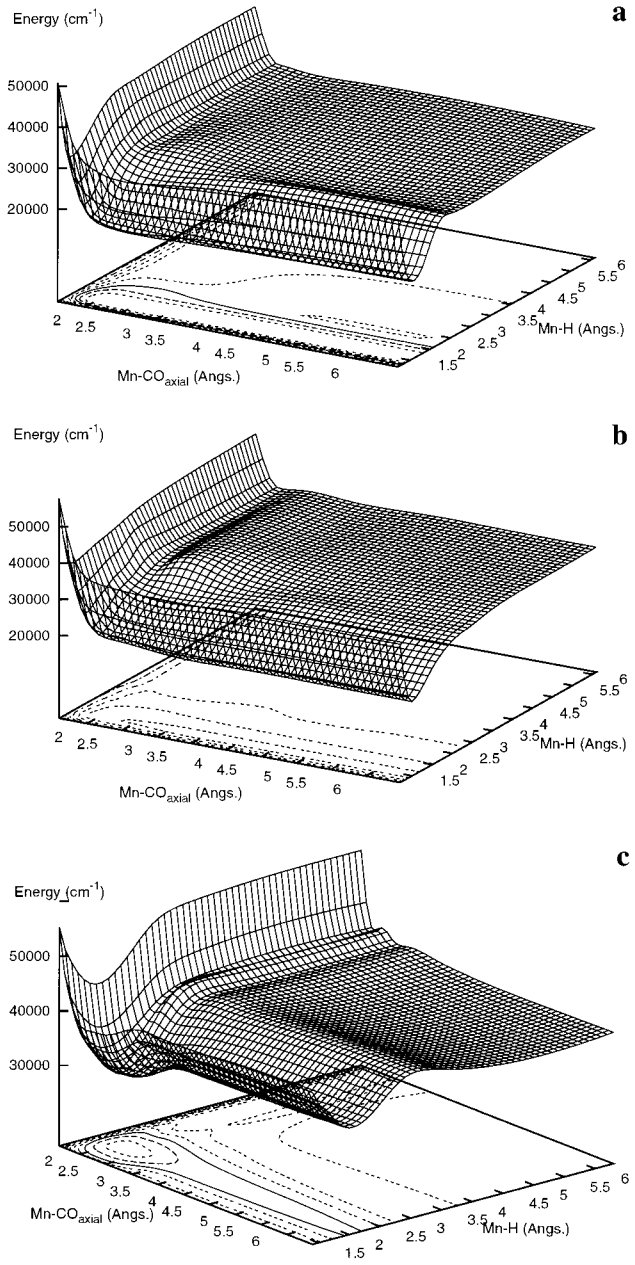

Figure 6. Two-dimensional CASSCF/MR-CCI potential energy surfaces as a function of $q_a = [Mn-H]$ and $q_b = [Mn-CO_{ax}]$ bond elongations for (a) the b^1A' (MLCT), (b) the c^1A' (MLCT), and (c) the e^1A' (SBLCT) excited states of $Mn(H)(CO)_3$(H-DAB).

of the different excited states and the probability of the Mn−H bond homolysis after 1 ps of propagation, respectively. After excitation to the d^1A' and e^1A' states ($V^{max}(d^1A'/e^1A') = 200$ cm^{-1}) 8% of the initial wave packet has enough energy to overcome the double-well potential (see Figure 4a) and dissociates toward the Mn−H bond homolysis primary products H + $Mn(CO)_3$(H-DAB) in less than 50 fs (Figure 11).

The rest of the system is trapped in the Franck−Condon region on the singlet states. According to the population of the low-lying triplet states after 1 ps of simulation the intersystem crossing processes are insignificant. One-dimensional simulation (along $q_b = [Mn-CO_{ax}]$) of the photodissociation dynamics after UV irradiation shows that this channel of deactivation is highly improbable. The initial wave packet prepared on the d^1A' and e^1A' coupled potentials oscillates between the two minima (see Figure 5a) as illustrated by the population evolution as a function of the time in Figure 12.

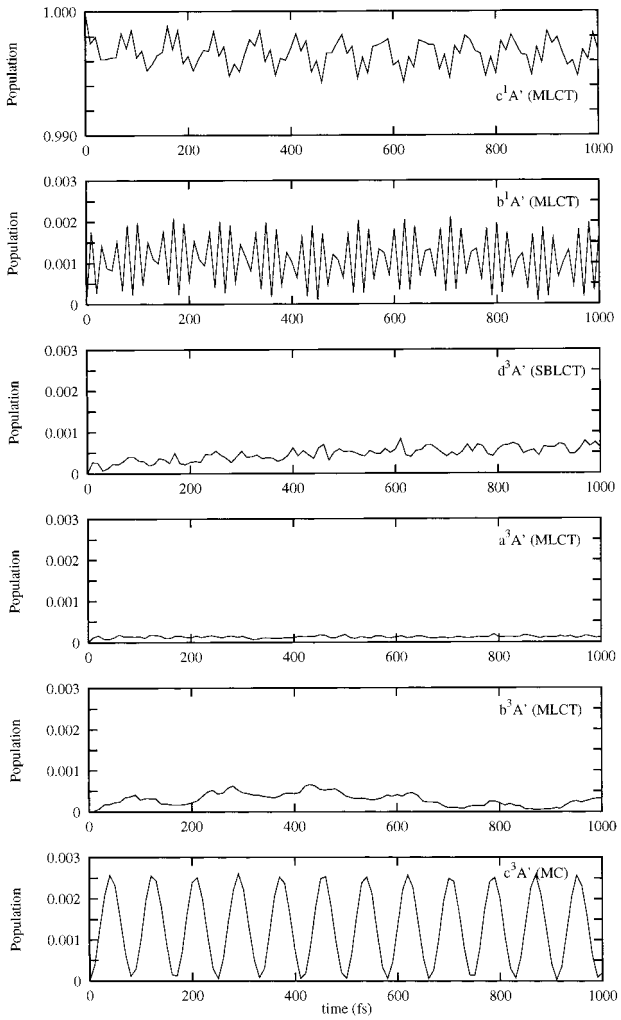

Figure 7. Evolution of the low-lying excited state population of Mn(H)(CO)$_3$(H-DAB) after irradiation in the visible as a function of time (along the q_a = [Mn−H] bond coordinate).

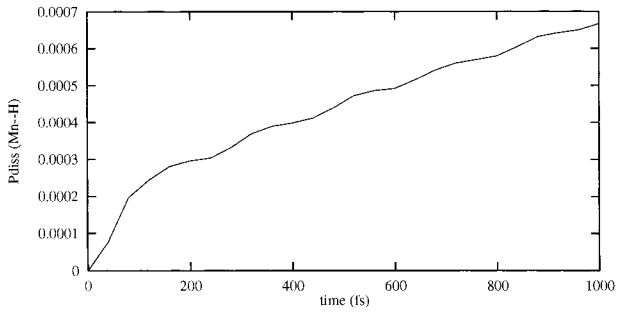

Figure 8. Probability of the Mn−H bond homolytic cleavage in Mn(H)(CO)$_3$(H-DAB) as a function of time after irradiation in the visible.

On the basis of these one-dimensional simulations results, the triplet states and the singlet excited states ranging in the UV energy domain have been excluded from the two-dimensional simulation and only the $V_{b^1A'}(q_a,q_b)$ and $V_{c^1A'}(q_a,q_b)$ potentials have been retained.

Two-Dimensional Simulation of the Photodissociation Dynamics after Absorption in the Visible. The time evolution of the system on the low-lying singlet MLCT states has been followed by propagation of the $\Psi_{b^1A'}(q_a,q_b,t)$ and $\Psi_{c^1A'}(q_a,q_b,t)$ wave packets on the $V_{b^1A'}(q_a,q_b)$ and $V_{c^1A'}(q_a,q_b)$ nonadiabatically

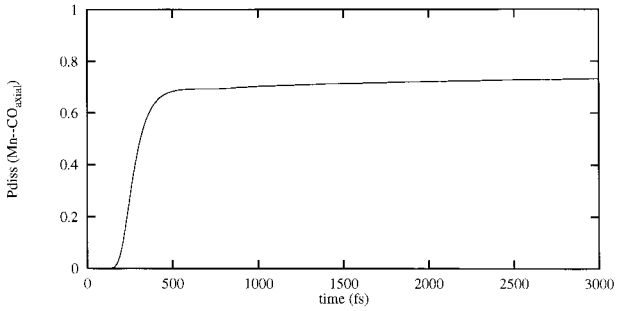

Figure 9. Probability of the axial CO loss in Mn(H)(CO)$_3$(H-DAB) as a function of time after irradiation in the visible.

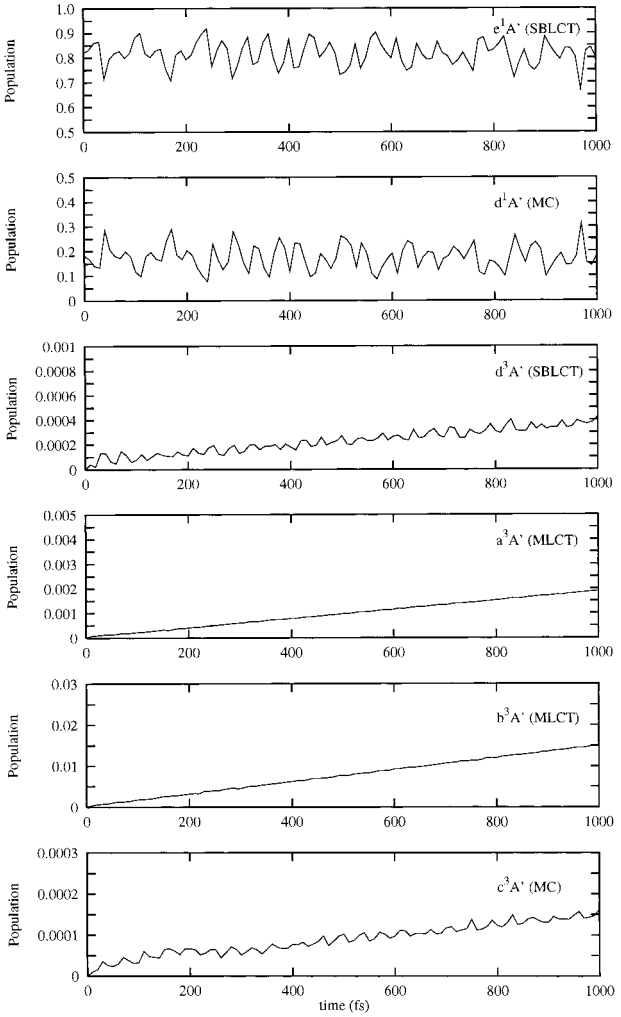

Figure 10. Evolution of the population of the low-lying excited states of Mn(H)(CO)$_3$(H-DAB) after irradiation in the UV as a function of time (along the q_a = [Mn−H] bond coordinate).

coupled potentials with the following initial conditions:

$$\Psi_{b^1A'}(q_a,q_b,t=0) = 0 \tag{18}$$

$$\Psi_{c^1A'}(q_a,q_b,t=0) = 1.0\Phi_{a^1A',0,0}(q_a,q_b) \tag{19}$$

After the a^{1}A′→ c^{1}A′ initial transition, the wave packet evolves in a very short time scale (<100 fs), as depicted in Figure 13, to the dissociation channel corresponding to the axial CO loss. This process is almost adiabatic.

The dissociation probability reaches 99% in 400 fs (Figure 14) and exceeds significantly the probability obtained from the one-dimensional simulation (70%). This direct and ultrafast

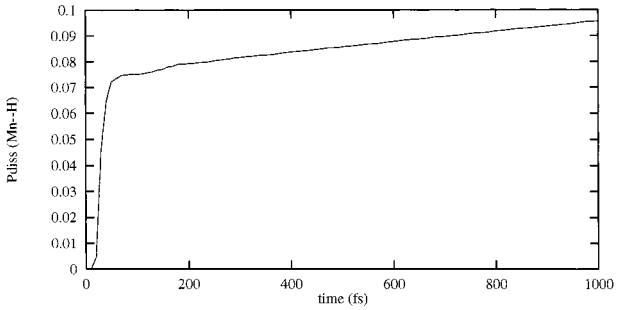

Figure 11. Probability of the Mn−H bond homolytic cleavage in Mn(H)(CO)$_3$(H-DAB) as a function of time after irradiation in the UV.

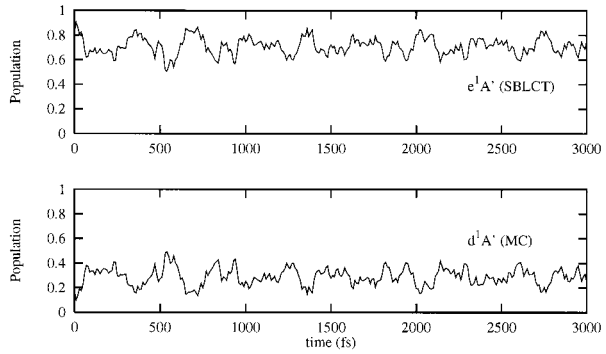

Figure 12. Evolution of the e^{1}A′ and d^{1}A′ excited state population after irradiation in the UV as a function of time (along the q_b = [Mn−CO_{ax}] bond elongation).

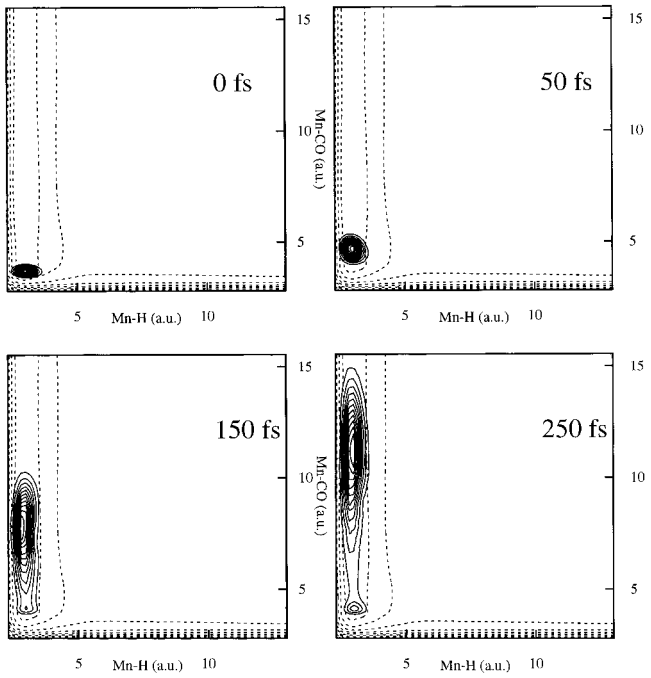

Figure 13. Time evolution of the $\Psi_{c^1A'}(q_a,q_b,t)$ wave packet on the $V_{c^1A'}(q_a,q_b)$ (dashed lines) potential.

channel of deactivation of Mn(H)(CO)$_3$(H-DAB) will be the only primary reaction observed after irradiation of the molecule in the visible energy domain.

IV. Conclusion

The photodissociation and electronic spectroscopy of Mn(H)(CO)$_3$(H-DAB), a model system for a series of α-diimine complexes, have been investigated through wave packet dynamics based on ab initio potentials calculated for the ground and

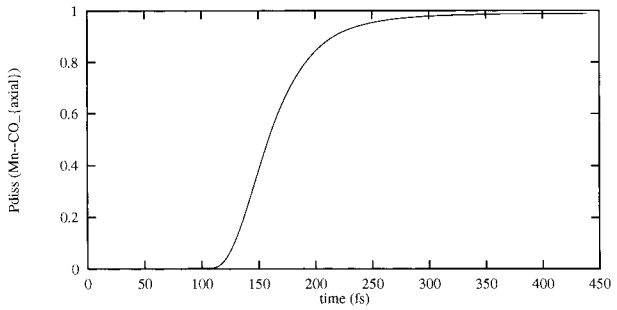

Figure 14. Probability of the axial CO loss in Mn(H)(CO)$_3$(H-DAB) as a function of time after irradiation in the visible (two-dimensional simulation).

low-lying excited states corresponding to MLCT, MC, and SBLCT transitions. Two reactive channels of deactivation of the molecules after irradiation either in the visible or in the UV energy domains have been considered, namely the metal−hydrogen bond cleavage leading to the diradicals H$^\bullet$ + $^\bullet$Mn(CO)$_3$(H-DAB) or the axial carbonyl loss, primary reactions currently observed in this class of complexes. According to the present simulation, performed in the picosecond time scale, the photodissociation mechanism is characterized by a direct and ultrafast (<500 fs) dissociation of the axial CO after initial excitation to the ^{1}MLCT state corresponding to the $3d_{xz} \rightarrow \pi^*_{H-DAB}$ excitation, calculated at 23 020 cm^{-1} with an oscillator strength of 0.39. This very efficient (70% and 99% in the one- and two-dimensional simulations, respectively) process should be the only primary reaction observed after irradiation of the molecule in the visible energy domain in agreement with the high quantum yields usually observed for this reaction in a number of Mn(R)(CO)$_3$(α-diimine) manganese complexes ($0.6 \leq \phi_{CO} \leq 1.0$, depending on the nature of the ligand R or of the α-diimine group) after irradiation at 500 nm. Nonradiative transitions to the triplet states or direct homolytic rupture of the metal−hydrogen bond are not competitive with this ultrafast primary reaction. This is a consequence of the nearly dissociative character of the MLCT potentials with respect to the Mn−CO_{ax} bond elongation due to the decrease of the dπ−pπ back-donation when going from the electronic ground state to the MLCT states. The only dissociative state along the Mn−H bond coordinate is the ^{3}SBLCT state corresponding to the $\sigma_{Mn-H} \rightarrow \pi^*_{H-DAB}$ excitation. Small values of spin−orbit coupling between this state and the low-lying ^{1}MLCT states (≤75 cm^{-1}) coupled with the presence of critical geometries (singlet−triplet crossings) at long distance of the Franck−Condon region (beyond 2.0 Å) make the homolytic cleavage of the Mn−H unlikely. A more favorable situation has been observed for the ethyl complex Mn(Et)(CO)$_3$(H-DAB),[42] where the intersystem crossing processes are more efficient, leading to a significant population of the triplet states (35%) in less than 1 ps. Consequently, the cleavage of the Mn−ethyl bond is more efficient than the Mn−H bond homolysis.

The shape of the potentials in the vicinity of the UV absorption essentially composed of two electronic states, namely the SBLCT and MC states corresponding to $\sigma_{Mn-H} \rightarrow \pi^*_{H-DAB}$ and 3d → 3d excitations, is responsible for the low photoreactivity of the Mn(H)(CO)$_3$(H-DAB) after UV irradiation. As developed elsewhere,[43] the rhenium analogue Re(H)(CO)$_3$(H-DAB) is characterized by a totally different photodissociation dynamics, essentially due to the occurrence of a very efficient ^{1}MLCT → ^{3}SBLCT intersystem crossing process in less than 500 fs.

(42) Guillaumont, D.; Daniel, C., to be submitted.
(43) Cote-Bruand, I.; Daniel, C., in preparation.

Accounting for other geometrical relaxation effects or solvent effects should lead to a less contrasted photochemical behavior but the main conclusions, namely the occurrence of a very efficient, direct, and ultrafast CO loss and an insignificant population of the triplet states in less than 1 ps, should not be affected by more refined treatments.

Acknowledgment. We thank Professor A. Vlcek and Professor D. J. Stufkens for stimulating discussions and Professor Ad Oskam for initiating this project. This work was undertaken as part of the European collaborative COST projects D4/0001/94 and D14/0001/99. We thank the Département de Chimie of the CNRS for specific COST financial support. The ab initio calculations have been carried out either on the Cray C98 computer and workstations at the IDRIS (Orsay, France) through a grant of computer time from the Conseil Scientifique or on the RS6000 workstations at the LCQS (Strasbourg, France).

JA992069G